

# The hunt for nonflammable refrigerant blends to replace R-134a<sup>☆</sup>

Ian H. Bell<sup>a,\*</sup>, Piotr A. Domanski<sup>b</sup>, Mark O. McLinden<sup>a</sup>, Gregory T. Linteris<sup>b</sup>

<sup>a</sup>*Applied Chemicals and Materials Division, National Institute of Standards and Technology, Boulder, CO, 80305, USA*

<sup>b</sup>*Energy and Environment Division, National Institute of Standards and Technology, Gaithersburg, MD, 20899, USA*

---

## Abstract

We investigated refrigerant blends as possible low GWP (global warming potential) alternatives for R-134a in an air-conditioning application. We carried out an extensive screening of the binary, ternary, and four-component blends possible among a list of 13 pure refrigerants comprising four hydrofluoroolefins (HFOs), eight hydrofluorocarbons (HFCs), and carbon dioxide. The screening was based on a simplified cycle model, but with the inclusion of pressure drops in the evaporator and condenser. The metrics for the evaluation were nonflammability, low GWP, high COP (coefficient of performance), and a volumetric capacity similar to the R-134a baseline system. While no mixture was ideal in all regards, we identified 16 binary and ternary blends that were nonflammable (based on a new estimation method) and with COP and capacity similar to the R-134a baseline; the tradeoff, however, was a reduction in GWP of, at most, 54% compared to R-134a. An additional seven blends that were estimated to be "marginally flammable" (ASHRAE Standard 34 classification of A2L) were identified with GWP reductions of as much as 99%. These 23 "best" blends were then simulated in a more detailed cycle model.

*Keywords:* refrigerant blends, flammability, cycle efficiency, alternatives to R-134a

---

## 1. Introduction

The medium-pressure hydrofluorocarbon (HFC) R-134a found application in a broad range of equipment following the phase-out of ozone depleting fluids; these include water chillers, air conditioners, and domestic and medium-temperature commercial refrigeration systems. Because of its impact on climate (global warming potential (GWP) of 1300), R-134a is one of the substances controlled by the Kigali Amendment to the Montreal Protocol (UNEP, 2016). The Amendment requires a significant reduction in the use of high-GWP fluids in air-conditioning and refrigeration equipment. Consequently, the use of R-134a must be curtailed.

Like all segments of society, the U.S. military is examining its options to reduce the global-warming-potential (GWP) footprint of its air-conditioning and refrigeration

systems. But while much of the refrigeration industry is considering a move to refrigerants that are flammable, or at least marginally flammable, the unique operating environments of many military systems demand nonflammable replacement refrigerants. The goal of this work was to identify nonflammable, but lower-GWP, replacements for R-134a in a baseline air-conditioning application while maintaining capacity and energy efficiency.

Significant research activity investigating R-134a replacement options was already in place within the Society of Automotive Engineers as early as 20 years ago (Brown, 2012). The four blends of great original interest carrying commercial names AC1-1, DP-1, Fluid H, and JDH, were all nonflammable. Eventually, these blends were abandoned due to either toxicity or stability concerns, and mildly-flammable R-1234yf became the dominant low-GWP fluid in mobile air conditioners (ACs) with R-744 (carbon dioxide) ACs having a small market share.

Independently of the introduction of R-1234yf and R-744 in mobile ACs, the study of low-GWP replacements for R-134a has remained an active research area. Numerous publications have presented experimental work that included medium-temperature refrigeration and air-conditioning operating regimes. In most cases, these studies considered fluids classified by ASHRAE Standard 34 or endorsed by chemical companies, both single-compound fluids (R-1234yf, R-1234ze(E), R-290, R-600a) and their blends. (i.e., Sánchez et al. (2017); Llopis et al. (2017); Mota-Babiloni et al. (2015, 2017); Wang (2014)). In a recent analytical study applicable to refrigeration, Gaurav and

---

<sup>☆</sup>Contribution of the National Institute of Standards and Technology, not subject to copyright in the U.S. Commercial equipment, instruments, or materials are identified only in order to adequately specify certain procedures. In no case does such identification imply recommendation or endorsement by the National Institute of Standards and Technology, nor does it imply that the products identified are necessarily the best available for the purpose. This work is adapted from paper 2110 presented at the 17<sup>th</sup> International Refrigeration and Air Conditioning Conference at Purdue, July 9-12, 2018 Bell et al. (2018)

\*Corresponding Author

*Email addresses:* [ian.bell@nist.gov](mailto:ian.bell@nist.gov) (Ian H. Bell), [piotr.domanski@nist.gov](mailto:piotr.domanski@nist.gov) (Piotr A. Domanski), [mark.mclinden@nist.gov](mailto:mark.mclinden@nist.gov) (Mark O. McLinden), [linteris@nist.gov](mailto:linteris@nist.gov) (Gregory T. Linteris)

## NOMENCLATURE

### Variables

|                  |   |
|------------------|---|
| $A$              | cross-sectional area ( $\text{m}^2$ )   |
| $A_r$            | surface area on the refrigerant side ( $\text{m}^2$ )                         |
| $C_{\Delta p}$   | pressure drop constant  |
| COP              | coefficient of performance (-)  |
| $D$              | diameter (m)  |
| $G$              | mass flux ( $\text{kg}^2 \cdot \text{s}^{-1} \cdot \text{m}^{-2}$ )           |
| $f_F$            | Fanning friction factor (-)   |
| GWP              | global warming potential (-)  |
| $h$              | mass specific enthalpy ( $\text{J} \cdot \text{kg}^{-1}$ )                    |
| $L$              | length (m)  |
| $\dot{m}$        | mass flow rate ( $\text{kg} \cdot \text{s}^{-1}$ )                            |
| $p$              | pressure (Pa)   |
| $\Delta p$       | pressure difference (Pa)  |
| $Q$              | capacity (W)  |
| $Q_{\text{vol}}$ | volumetric capacity ( $\text{W} \cdot \text{m}^{-3}$ )                        |
| $R$              | heat-transfer resistance ( $\text{K} \cdot \text{W}^{-1}$ )                   |
| $s$              | mass specific entropy ( $\text{J} \cdot \text{kg}^{-1} \cdot \text{K}^{-1}$ ) |
| $\Delta T$       | temperature difference (K)  |
| $T$              | temperature (K)   |
| UA               | overall heat conductance ( $\text{W} \cdot \text{K}^{-1}$ )                   |

|            |   |
|------------|---|
| $\alpha_r$ | refrigerant heat-transfer coefficient ( $\text{W} \cdot \text{m}^2 \cdot \text{K}^{-2}$ ) |
| $\mu''$    | viscosity of saturated vapor (Pa·s)   |
| $\rho$     | mass density ( $\text{kg} \cdot \text{m}^{-3}$ )  |
| $\rho''$   | mass density of saturated vapor ( $\text{kg} \cdot \text{m}^{-3}$ )                       |
| $\eta_a$   | adiabatic efficiency (-)  |

### Subscripts

|        |                                 |
|--------|---------------------------------|
| ad     | adiabatic flame temperature     |
| bub    | bubble point                    |
| c      | critical                        |
| dew    | dew point                       |
| cond   | condenser                       |
| evap   | evaporator                      |
| hx     | heat exchanger                  |
| r      | refrigerant                     |
| vol    | volumetric                      |
| sc     | subcooling                      |
| sh     | superheat                       |
| 1-4    | state points                    |
| 2s     | isentropic compression          |
| 1*, 2* | state points with pressure drop |

Kumar (Gaurav and Kumar, 2018), examined 31 fluids, which included binary and ternary blends of R-134a, R-1234yf, and R-1234ze(E). In their work, the flammability of the examined fluids was based on their ASHRAE Standard 34 classification, where available.

In the current study, we evaluated binary, ternary and four-component blends possible among a list of 13 refrigerants comprising four hydrofluoroolefins (HFOs), eight hydrofluorocarbons (HFCs), and carbon dioxide (R-744) in search of best-performing non-flammable substitute for R-134a in an air-conditioning application. The flammability of each blend was estimated using a novel method formulated within this study Linteris et al. (2019, under revision). Performance merits of the selected 23 “best” fluids were determined using an advanced cycle model, which optimized refrigerant circuitry for each fluid in the evaporator and condenser and maintained the same heat flux in the evaporator for all fluids, a prerequisite for fair evaluation of competing fluids in a refrigeration cycle (McLinden and Radermacher, 1987).

The selection of a refrigerant blend to replace refrigerant R-134a is a multi-objective optimization process. There are several desired objectives:

- **Minimize/eliminate flammability:** As discussed in Linteris et al. (2018), the combination of the adiabatic flame temperature and the F-substitution ratio yields a prediction of the flammability class (1, 2L, 2, 3) according to the ASHRAE 34 standard (ASHRAE, 2016). It is preferred to have a flammability class designation of 1 (“no flame propagation”), but as demonstrated below, enforcing that the blend be nonflammable comes at the cost of a lower system

efficiency and/or a higher GWP.

- **Minimize GWP:** The GWP of a blend is defined as the mass-fraction-weighted GWP of the blend’s components. Several time horizons are possible for the calculation of GWP, but it is most common to consider a 100-year time horizon. The 100-year GWP values for pure fluids are tabulated in a number of sources, and here we used the values from the UN IPCC report (Myhre et al., 2013).
- **Maximize COP:** the coefficient of performance, or COP, characterizes the efficiency of the system. The larger the COP, the better the system efficiency.
- **Match the volumetric capacity  $Q_{\text{vol}}$  of the baseline R-134a system.** The  $Q_{\text{vol}}$  is a figure of merit that is related to the size of the compressor needed to achieve a given cooling capacity. The larger the  $Q_{\text{vol}}$ , the smaller the compressor needs to be for a given cooling capacity.

Our search for optimal R-134a replacement blends involved the above four figures of merit and consisted of the following steps:

1. Selection of pure refrigerants of low toxicity and zero ODP that could possibly form a replacement blend.
2. Determination of flammability classification, GWP, COP, and  $Q_{\text{vol}}$  for an exhaustive matrix of possible binary and ternary mixture compositions. In a separate analysis, the screening was expanded to also include all four-component mixture compositions. In this step, we evaluated COP and  $Q_{\text{vol}}$  using a simplified cycle model.

3. Selection of "best" blends based on the figures of merit of the blends.
4. Determination of COP and  $Q_{\text{vol}}$  of the "best" blends using an advanced cycle model.

## 2. Fluid Selection

Based on a comprehensive search of chemical compounds that could serve as working fluids in air-conditioning systems, McLinden et al. (2017) demonstrated that there are very limited options for low-GWP refrigerants. They identified the best working fluids based on assessments of their environmental impact, safety, performance characteristics, stability, and toxicity. But no single-component refrigerant was ideal in all respects; that is, no fluid was simultaneously nonflammable, low-GWP, and with good performance in an air-conditioning system. Thus, in this study, we turn to blends.

For blending, we selected 13 fluids within a range of pressure, flammability, and GWP values that might produce a blend with the desired characteristics of a R-134a replacement. These included hydrofluoroolefins (HFOs), which have very low GWP values ( $\approx 1$  relative to  $\text{CO}_2$ ), but that are mildly flammable; hydrofluorocarbons (HFCs) with moderate-to-high GWP values that were nonflammable and thus, might serve to suppress the flammability of a blend; additional mildly flammable HFCs; and carbon dioxide ( $\text{CO}_2$ ), which is nonflammable with  $\text{GWP} \equiv 1$ , but which would raise the working pressure of a blend. All the selected fluids were of low toxicity (*i.e.*, an "A" classification under ASHRAE Standard 34 (ASHRAE, 2016)). Additional considerations were the commercial availability of the fluid and the availability of property data (in the form of an accurate equation of state), so that cycle simulations could be carried out with some measure of confidence.

The list of candidate working fluids considered in this study is summarized in Table 1.

## 3. Estimated Figures of Merit of the Blends

### 3.1. Simplified Cycle Model

The cycle model is based upon a simplified analysis of a four-component air conditioning system with lumped pressure drops. A schematic of the system is shown in Fig. 1, and  $\log(p)$ - $h$  and  $T$ - $s$  property figures are shown in Fig. 2. Due to the subtle complexities of modeling blends in thermodynamic cycles, we describe the cycle model in detail below. The specification of the model parameters is as follows:

- Evaporator dew-point temperature  $T_{\text{evap,dew}}$ : 10 °C
- Condenser bubble-point temperature  $T_{\text{cond,bub}}$ : 40 °C
- Evaporator outlet superheat  $\Delta T_{\text{sh}}$ : 5 K
- Condenser exit subcooling  $\Delta T_{\text{sc}}$ : 7 K

- Compressor adiabatic efficiency  $\eta_a$ : 0.7
- Evaporator pressure drop: for the baseline system, a reduction in dew-point temperature of 2 K
- Condenser pressure drop: for the baseline system, a reduction in bubble-point temperature of 2 K

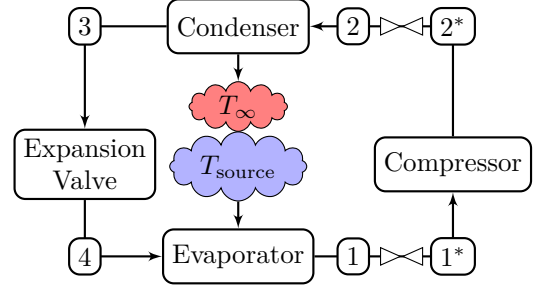


Figure 1: System schematic. The state point indices 1, 2, etc. correspond to the labeled state points in Fig. 2.

The key difference between this cycle model and other simplified cycle models is the inclusion of a simplified pressure drop model. It is assumed that the pressure drop from the high-side components and the low-side components can be lumped into pressure drops at the outlet and inlet of the compressor, respectively. Therefore the compressor sees a larger pressure lift than the pressure ratio corresponding to the pressures in the evaporator and condenser. The drops in saturation temperature for high- and low-sides of the system are specified for the baseline R-134a system, and the pressure drop scaling (described below) is used to calculate the pressure drop for the refrigerant blends.

In the simplified cycle analysis, the pressures in the evaporator and the condenser are assumed to be constant, given by vapor-liquid equilibrium calculations at the respective saturation pressure

$$p_{\text{evap}} = p_{\text{dew}}(T_{\text{evap,dew}}) \quad (1)$$

$$p_{\text{cond}} = p_{\text{bub}}(T_{\text{cond,bub}}). \quad (2)$$

The selection of the saturation states used to define the low- and high-side pressures is based on a rudimentary pinch analysis. This pinch analysis assumes that the source and sink temperatures are fixed, that the condenser outlet pinch is fixed, and that the evaporator outlet pinch is fixed. Therefore, stacking up the temperature differences (plus the respective superheating or subcooling), we can arrive at the relevant saturation temperature. This method is the worst-case simplified cycle analysis option for mixtures with temperature glide (McLinden and Radermacher, 1987) because the heat-transfer irreversibilities are maximized. This represents a conservative approach in the sense that it favors drop-in replacements that would require little or no modifications of existing systems. For blends having significant temperature glide, and systems

Table 1: Pure fluids selected in this study and some of their characteristics. The GWP<sub>100</sub> values are from the UN IPCC report (Myhre et al., 2013) ( $T_c$ : critical temperature;  $\bar{\Pi}$ : normalized flammability metric from Eq. (19) with the initial temperature of the reactants of 60 °C and mole fraction of H<sub>2</sub>O in the air of 0.014)

| ASHRAE designation | long name                        | formula                            | $T_c/K$ | GWP <sub>100</sub> | ASHRAE classification | $\bar{\Pi}$ |
|--------------------|----------------------------------|------------------------------------|---------|--------------------|-----------------------|-------------|
| R-134a             | 1,1,1,2-tetrafluoroethane        | CF <sub>3</sub> CH <sub>2</sub> F  | 374.2   | 1300               | A1                    | -10.5       |
| R-227ea            | 1,1,1,2,3,3,3-heptafluoropropane | CF <sub>3</sub> CHFCF <sub>3</sub> | 374.9   | 3350               | A1                    | -38.6       |
| R-125              | perfluoroethane                  | CHF <sub>2</sub> CF <sub>3</sub>   | 339.2   | 3170               | A1                    | -37.7       |
| R-143a             | 1,1,1-trifluoroethane            | CF <sub>3</sub> CH <sub>3</sub>    | 345.9   | 4800               | A2L                   | 26.7        |
| R-32               | difluoromethane                  | CH <sub>2</sub> F <sub>2</sub>     | 351.3   | 677                | A2L                   | 34.1        |
| R-152a             | 1,1-difluoroethane               | CHF <sub>2</sub> CH <sub>3</sub>   | 386.4   | 138                | A2                    | 54.8        |
| R-134              | 1,1,2,2-tetrafluoroethane        | CHF <sub>2</sub> CHF <sub>2</sub>  | 391.8   | 1120               | Not assigned          | -6.4        |
| R-41               | fluoromethane                    | CH <sub>3</sub> F                  | 317.3   | 116                | Not assigned          | 67.6        |
| R-1234yf           | 2,3,3,3-tetrafluoropropene       | CF <sub>3</sub> CF=CH <sub>2</sub> | 367.9   | 1                  | A2L                   | 4.8         |
| R-1234ze(E)        | trans-1,3,3,3-tetrafluoropropene | CHF=CHCF <sub>3</sub> (trans)      | 382.5   | 1                  | A2L                   | 4.8         |
| R-1234ze(Z)        | cis-1,3,3,3-tetrafluoropropene   | CHF=CHCF <sub>3</sub> (cis)        | 423.3   | 1                  | Not assigned          | 4.8         |
| R-1243zf           | 3,3,3-trifluoropropene           | CH <sub>2</sub> =CHCF <sub>3</sub> | 376.9   | 1                  | Not assigned          | 43          |
| R-744              | carbon dioxide                   | CO <sub>2</sub>                    | 304.1   | 1                  | A1                    | N.A.        |

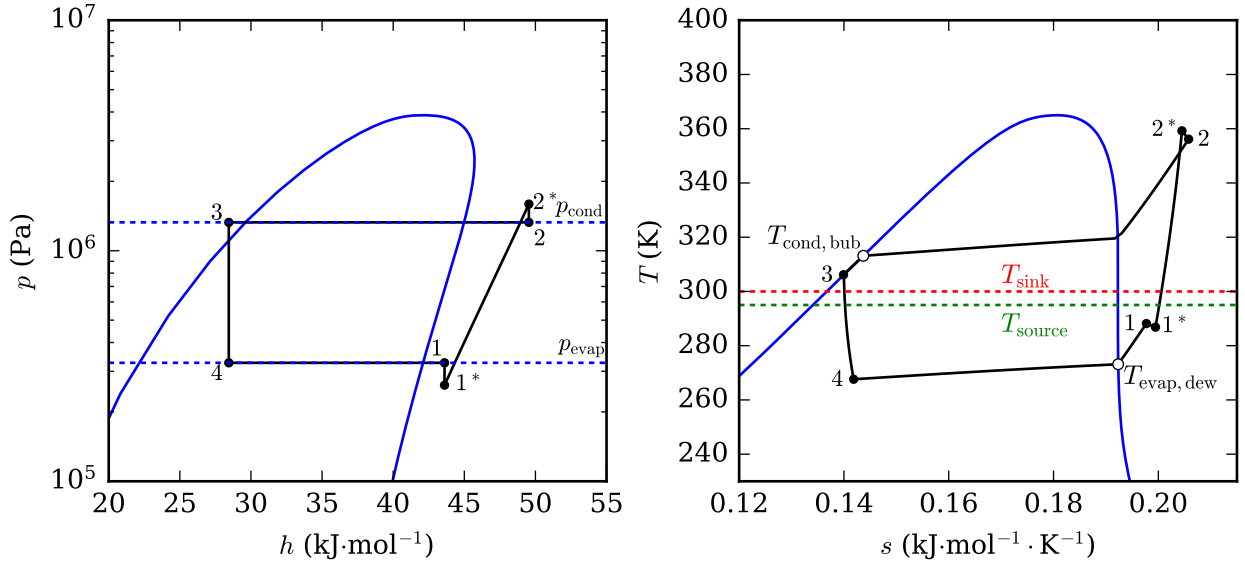


Figure 2: Schematic  $p$ - $h$  and  $T$ - $s$  cycle diagrams for an equimolar mixture of R-125 + R-1234ze(E). Calculations are carried out with NIST REFPROP (Lemmon et al., 2018) called by the CoolProp interface (Bell et al., 2014).

with counterflow or cross-counterflow heat exchange, the temperature profiles of the source and sink fluids and that of the working mixture may be better aligned, resulting in lower heat transfer irreversibilities and higher efficiencies.

*Condenser.* The outlet enthalpy of the condenser is given by

$$h_3 = h(T_3, p_{\text{cond}}), \quad (3)$$

where the outlet temperature of the condenser  $T_3$  is given by

$$T_3 = T_{\text{cond,bub}} - \Delta T_{\text{sc}}, \quad (4)$$

and where the bubble-point temperature of the condenser is given by

$$T_{\text{cond,bub}} = T_{\text{bub}}(p_{\text{cond}}). \quad (5)$$

The pressure drop in the condenser ( $\Delta p_{\text{high}}$ ) is given by Eq. (17), in which  $\rho''$  and  $\mu''$  are evaluated at the dew point at the condensing pressure  $p_{\text{cond}}$ .

*Evaporator.* The dew-point temperature is imposed for the evaporator, as is its inlet enthalpy (because the outlet state of the condenser is fully specified and the throttling process is assumed to be adiabatic). Therefore the states 3, 4, and 1 can be fully specified and the enthalpies calculated from

$$h_4 = h_3 \quad (6)$$

$$h_1 = h(T_{\text{evap}} + \Delta T_{\text{sh}}, p_{\text{evap}}) \quad (7)$$

The pressure drop in the evaporator  $\Delta p_{\text{low}}$  is given by the relationship in Eq. (17), in which  $\rho''$  and  $\mu''$  are evaluated at the dew point at the evaporation pressure  $p_{\text{evap}}$ .

*Compressor.* The pressure drops in the cycle are lumped at the compressor; the pressure drop in the low-pressure components reduces the suction pressure of the compressor and the pressure drop in the high-pressure components increases the discharge pressure of the compressor. Therefore, the inlet state of the compressor  $1^*$  is given by the isenthalpic pressure drop relative to the state point 1:

$$h_{1^*} = h_1 \quad (8)$$

$$T_{1^*} = T(h_{1^*}, p_{\text{evap}} - \Delta p_{\text{low}}) \quad (9)$$

Similarly, the outlet pressure of the compressor  $p_{2^*}$  is given by  $p_{2^*} = p_{\text{cond}} + \Delta p_{\text{high}}$ . The classical adiabatic efficiency formulation is used for the compressor, assuming that there is no heat transfer from the compressor to the environment. Therefore, the adiabatic efficiency is defined by

$$\eta_a = \frac{h_{2s} - h_{1^*}}{h_{2^*} - h_{1^*}}, \quad (10)$$

where the isentropic enthalpy  $h_{2s}$  is obtained from

$$h_{2s} = h(s_{1^*}, p_{2^*}). \quad (11)$$

*Cycle metrics.* The COP of the air conditioner is given by

$$\text{COP} = \frac{h_1 - h_4}{h_{2^*} - h_{1^*}} \quad (12)$$

and the volumetric capacity of the heat pump is given by

$$Q_{\text{vol}} = (h_4 - h_1) \cdot \rho(T_{1^*}, p_{1^*}). \quad (13)$$

*Pressure drop modeling.* As demonstrated by McLinden et al. (2017), the inclusion of pressure drop in the model (even if highly approximate), is crucial to yield a fair screening of refrigerants. The simplified pressure drop in our analysis is based upon scaling the system for the refrigerant blends to have the same capacity as the baseline R-134a system.

Although pressure drops are lumped at the compressor, they are based on the frictional pipe flow analysis of a homogeneous fluid applied to the evaporator and condenser (making use of the Fanning friction factor of turbulent flow and neglecting accelerational pressure drop) given by

$$\Delta p = \frac{2f_{\text{F}}G^2L}{\rho D}, \quad (14)$$

where

$$f_{\text{F}} = 0.046 \left( \frac{GD}{\mu} \right)^{-0.2}. \quad (15)$$

The pressure drop for a refrigerant blend is calculated from

$$\Delta p = C_{\Delta p} \frac{(\mu'')^{0.2}}{\rho''(h_1 - h_4)^{1.8}} \quad (16)$$

where  $C_{\Delta p}$  is a heat-exchanger-specific pressure-drop coefficient obtained by imposing the equality of cooling capacity  $Q = \dot{m} \cdot (h_1 - h_4)$  and lumping all non-thermophysical properties into the constant  $C_{\Delta p}$ . The parameter  $C_{\Delta p}$  captures the effective sizing of the heat exchanger for a given capacity. In these calculations, density  $\rho''$  and viscosity  $\mu''$  were evaluated at the dew-point state at the heat exchanger pressure. The coefficient  $C_{\Delta p}$  was obtained for the baseline R-134a system with pressure drop as described in Section 3.1, yielding the parameters

$$C_{\Delta p} = \Delta p_{\text{R-134a}} \frac{\rho''_{\text{R-134a}}(h_1 - h_4)_{\text{R-134a}}^{1.8}}{(\mu''_{\text{R-134a}})^{0.2}}, \quad (17)$$

with one coefficient for the evaporator, and another for the condenser.

### 3.2. Estimation of Flammability

The refrigerant flammability prediction of Linteris et al. (2018) uses two parameters that can be readily evaluated: the adiabatic flame temperature  $T_{\text{ad}}$  and the ratio of the number of fluorine atoms to the total of fluorine plus hydrogen atoms in the refrigerant blend,  $F/(F + H)$ .  $T_{\text{ad}}$  is calculated from the enthalpy of the reactants and products from Cantera (Goodwin et al., 2017), an open-source software package for problems involving chemical kinetics,

thermodynamics, and transport properties. The  $F/(F + H)$  ratio is calculated from the chemical formulas of the combustion reactants: the refrigerant blend plus humid air. A plot of  $T_{\text{ad}}$  versus  $F/(F+H)$  is constructed, with each point representing a refrigerant or blend, as shown in Fig. 3. Less flammable compounds are in the lower right of the plot, and more flammable, the upper left. The flammability of the refrigerant is represented by the slope of the line between an origin (at  $(F/(F + H)) = 0$  and  $T_{\text{ad}} = 1600$  K) and the point in question. The origin point is based on the observation that hydrocarbons (for which  $(F/(F + H)) = 0$ ) do not burn when diluted with an inert gas, or cooled, such that their adiabatic flame temperature falls below 1600 K. For more details, please see Linteris et al. (2018).

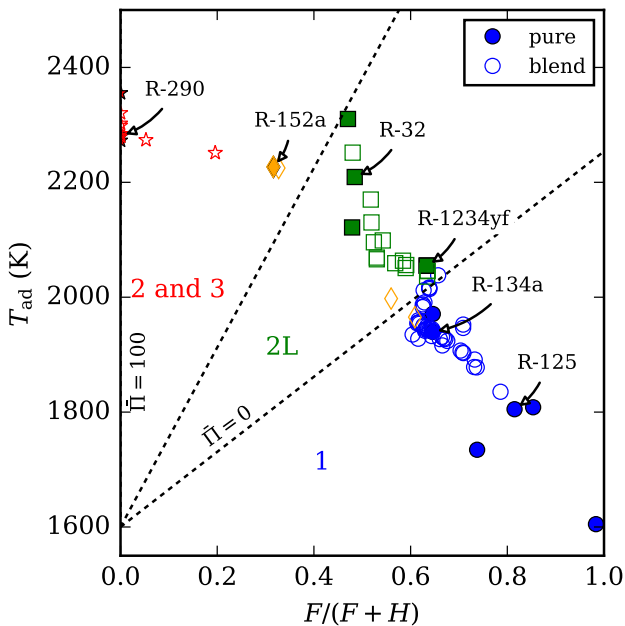


Figure 3: Estimation of flammability based on adiabatic flame temperature  $T_{\text{ad}}$  and  $F/(F+H)$  for pure fluids and blends, and flammability rating as specified in the ASHRAE 34 standard (ASHRAE, 2016). The colors correspond to the flammability class – 1: blue, 2L: green, 2: orange, 3: red. The initial temperature of the reactants is 60 °C.

Figure 3 shows the assessment of pure fluids and blends having an ASHRAE 34 classification. The values of  $T_{\text{ad}}$  and  $F/(F + H)$  are evaluated for mixtures at their nominal blend compositions. The dashed lines separate the ASHRAE Standard 34 flammability classes 1, 2L, and the combination of 2 and 3. As indicated, the present flammability estimation appears to represent the ASHRAE 34 data reasonably well.

The flammability index  $\Pi$  is defined as the angle swept from the lower right of the figure to the upper left, about the point  $(0, 1600$  K), or:

$$\Pi = \arctan2\left(\frac{T_{\text{ad}} - 1600}{2500 - 1600}, \frac{F}{F + H}\right) \times \frac{180}{\pi} \quad (18)$$

where  $\arctan2(y, x)$  gives the four-quadrant arctangent angle in the domain  $[-\pi, \pi]$ , and the angle is then shifted to  $[-180, 180]$ . We define the flammability boundary between classes 1 and 2L as  $\Pi_{1,2L} \equiv 36$ , though the precise value comes with significant uncertainty. This value is selected as a conservative value ensuring that only non-flammable mixtures are considered to be non-flammable. A normalized flammability index  $\bar{\Pi}$  is then defined by

$$\bar{\Pi} = \frac{\Pi - \Pi_{1,2L}}{90 - \Pi_{1,2L}} \times 100 \quad (19)$$

This results in a normalized flammability index  $\bar{\Pi}$  which is zero at the 1/2L boundary and 100 for the highly flammable hydrocarbons. Values less than zero indicate that the mixture is probably nonflammable according to the ASHRAE Standard 34 criteria. For more information, see Linteris et al. (2018).

For the flammability prediction, the uncertainty in the  $T_{\text{ad}}$  and  $F$  substitution rate are small, less than 1 %. For the predicted flammability class, there is large uncertainty near the 1/2L boundary. The main sources of uncertainty are estimated to be the accuracy of the underlying flammability database upon which the flammability predictive tool was developed, the effects of stretch on flammability limits, and molecular structure effects not accounted for in  $T_{\text{ad}}$  and the  $F$  substitution rate. These are discussed in more detail in Linteris et al. (Linteris et al., 2018). Finally, flammability limits are generally device-dependent (Takahashi et al., 2003), so while the current approach can predict the behavior of a mixture in the modified ASTM E-681 (for constituents which are chemically similar to those used to develop the model; i.e., HCs, HFCs, HFOs, etc.), the behavior of the mixtures in other flammability tests or actual full-scale configurations having more powerful ignition sources, clutter, turbulence, etc., may not be predicted as well by their behavior in the E-681 test.

### 3.3. Screening Results

The screening involved an extensive evaluation, using the simplified cycle model described in Section 3.1, of all possible combinations of the 13 fluids listed in Table 1 taken two or three at a time (*i.e.*, all possible binary and ternary mixtures). A composition interval of 0.04 mole fraction was applied to yield a total of 100,387 mixtures to be evaluated. The simplified cycle calculations were carried out in parallel in Python with the multiprocessing Python package<sup>1</sup>. The analysis of Linteris et al. (2018) was then applied to estimate the flammability class of the blend. The code used to carry out the calculations is available in the supplemental material.

The screening resulted in a large dataset of binary and ternary blends formed of the 13 components in Table 1 with an assessment of the figures of merit for each blend:

<sup>1</sup><https://docs.python.org/3/library/multiprocessing.html>

GWP, flammability index, and the COP and  $Q_{\text{vol}}$  from simplified cycle simulations. The production of this set of data was, in some sense, the easy part of this study; much more difficult was the determination of the “best” refrigerant blend(s). In truth, the selection of the “best” blend depends largely on how the user weights the available figures of merit.

Figure 4 provides a global overview of the results for the mixtures formed of the 13 components in Table 1. This figure presents a scatter plot of the COP versus  $Q_{\text{vol}}$  results for the studied blends sorted into nine “bins” of GWP and flammability. Additional blends had  $\text{GWP} > 1300$  and are not shown in Fig. 4. In the upper left hand corner of the figure are mixtures that are probably nonflammable according to the flammability assessment of Linteris et al. (2018) and have a  $\text{GWP} < 150$ , *i.e.*, less than 12% that of refrigerant R-134a. Figure 5 shows a graphical representation of the prevalence of each component in the different bins. The larger the radius of a wedge, the more prevalent the component is in the mixtures in that bin. In many of the bins there are certain components (or a family of components, *e.g.*, the HFOs) that dominate the bin. For instance, the low-GWP, nonflammable bin is dominated by carbon dioxide (R-744), and the low-GWP, moderately flammable bin is dominated by the HFOs. Each time a component occurs in a bin, its mole fraction in the mixture is added to the running sum for that bin. The mole-fraction-weighted prevalences are then normalized within the bin in order to yield the relative prevalence of each component.

Figure 6 presents another overview of the simulation results (COP versus GWP) where the emphasis is now placed on the mixtures that are on the margin between “flammable” and “non-flammable” according to the flammability estimation of Linteris et al. (2018). The results are sorted into four flammability ranges based on the flammability index defined in Section 3.2:  $10 < \bar{\Pi} < 45$  corresponds to likely class 2L fluids somewhat distant from the borderline region between ASHRAE flammability classes 1 and 2L;  $0 < \bar{\Pi} < 10$  is near, but on the flammable side of the flammability boundary (ASHRAE class 2L);  $-10 < \bar{\Pi} < 0$  is near the flammability boundary, but is likely nonflammable (ASHRAE class 1), and  $-100 < \bar{\Pi} < -10$  corresponds to more likely “non-flammable” (also ASHRAE class 1). Note that we plot only those blends with  $\text{GWP} < 1300$ , *i.e.*, less than that of R-134a, but otherwise Fig. 6 shows all of the blends simulated. If more flammable blends with ASHRAE flammability classification 2L are acceptable, the  $10 < \bar{\Pi} < 45$  could be further explored; the decision to cut off the marginally flammable bin at  $\bar{\Pi} = 10$  was motivated by the desire to find non-flammable refrigerant blends.

Several general trends and conclusions can be observed in Fig. 6. First, all the clearly nonflammable blends ( $-100 < \bar{\Pi} < -10$ ) have very low COPs compared to R-134a. Many of these blends contain a significant fraction of  $\text{CO}_2$ . Among the blends with  $-10 < \bar{\Pi} < 0$  (*i.e.*, the

blends that are likely class 1), there is a clear lower limit of  $\text{GWP} \approx 550$ ; this corresponds to a R-134a composition of about 45 mole %. This is the minimum fraction of R-134a necessary to suppress the flammability of R-1234yf or R-1234ze(E). (Other nonflammable fluids, such as R-125 or R-227ea, could serve to suppress flammability, but these have higher GWP values.) There is a general trend of the upper limit of COP increasing with GWP and with flammability. This is not a fundamental trade-off, but is a consequence of the nature of the very-low-GWP HFO refrigerants: the HFOs are more complex molecules compared to the corresponding HFCs that they are intended to replace, and this molecular complexity carries a performance penalty in the vapor-compression cycle.

Figure 7 zooms into the regions of most interest in Fig. 6, namely the blends with  $\text{COP} > 5$  in the middle two flammability ranges. This figure plots COP versus GWP and also indicates the composition and flammability index—see figure caption. The left panel ( $0 < \bar{\Pi} < 10$ ) is plotted only up to  $\text{GWP} = 500$ ; while there are many blends in this flammability range with higher values of GWP they would be of limited interest. There are patterns observed in Fig. 7 corresponding to “families” of blends with similar components and compositions that vary in even increments. The upper limit of COP in the right panel corresponds, in most cases, to the R-134a/1234yf binary blend (indicated by the heavy black symbols), and this binary continues into the left panel. An example is indicated by the shaded area in the left panel of Fig. 7. Starting with the R-134a/1234yf binary with composition (0.24/0.76), replacing R-1234yf with R-152a (shown with circles) increases the COP, but also increases the flammability (as indicated by color shifting towards yellow) until a flammability index of just less than  $\approx 10$  is reached at a R-152a content of 0.20 mole fraction at a constant R-134a content. The GWP also increases as R-1234yf ( $\text{GWP} \approx 1$ ) is replaced with R-152a ( $\text{GWP} = 138$ ). Returning to the R-134a/1234yf binary, replacing R-1234yf with R-1234ze(E) (shown with “+”) decreases the COP, but the GWP and flammability are little affected, since R-1234yf and R-1234ze(E) have identical molecular weights and similar estimated GWP and flammability. Note, however, that R-1234yf and R-1234ze(E) have slightly different measured flammability limits, which is not captured by the present simplified flammability screening tool (Kondo et al., 2012). Again returning to the R-134a/1234yf binary, replacing R-1234yf with R-1243zf (shown with pentagons) results first in an increase in COP and then a decrease as the R-1243zf content increases; the GWP values increase slightly because of the different molecular weights. Here the flammability increases significantly as the R-1243zf content increases.

### 3.4. Four-component Blends

The above analysis focused on the investigation of two and three component blends to replace refrigerant R-134a. In practice there is nothing that precludes the use of a

multi-component mixture; there are a number of four or more component mixtures included in the ASHRAE 34 standard. Therefore, we also investigated the potential to use four component mixtures.

The simulation of four component mixtures with 13 possible pure fluid constituents and an increment in mole fraction of 0.04 ( $=1/25$ ) results in a significant number of potential blends (1.4 million 4-component blends). In order to control the amount of data generated by the screening, results for which the COP was less than 4, or the  $\text{GWP}_{100}$  was greater than 1300, or  $F/(F+H)$  was less than 0.55 were culled (in the four component case only). This leaves only results for blends that have a good potential of being as good as, or better than, R-134a.

The simulations were carried out with the same Python code as above, and the results are available in the supplemental material. In short, there were no four-component mixtures that were obviously superior to the two- and three-component mixtures described above, though we include this analysis for completeness. The graphical representation of the results is also available in the supplemental material, as are the raw results in tabular (comma-separated-value) form.

### 3.5. Selection of "Best" Blends

We were not able to identify any blends that met all of our desired constraints. The mixtures in the non-flammable/low GWP bin (upper-left corner of Fig. 4) meet two of the desired objectives, but they suffer from a much lower efficiency than the baseline R-134a system and were dropped from further consideration. Thus, to define the "best" blends we selected the nonflammable blends having the highest COP within a range of GWP values from 537 to 870 (*i.e.*, from the remaining two bins in the left column of Fig. 4). These 16 "best blends" are listed in Table 2. Note that we did not separately select blends having very similar compositions to the "best" blends unless they offered a distinct advantage in one or more of our metrics.

If one is willing to tolerate a probable 2L flammability classification according to the ASHRAE 34 standard, there are low GWP options that yield efficiency near that of the baseline R-134a system (*i.e.*, the top two rows of the middle column in Fig. 4). We also selected seven additional blends that were marginally flammable with GWP values ranging from 8 to 498. The complete set of results obtained are presented in the supplemental material so that another user-desired screening could be readily applied. All this is to say that the search for the "perfect" refrigerant blend continues.

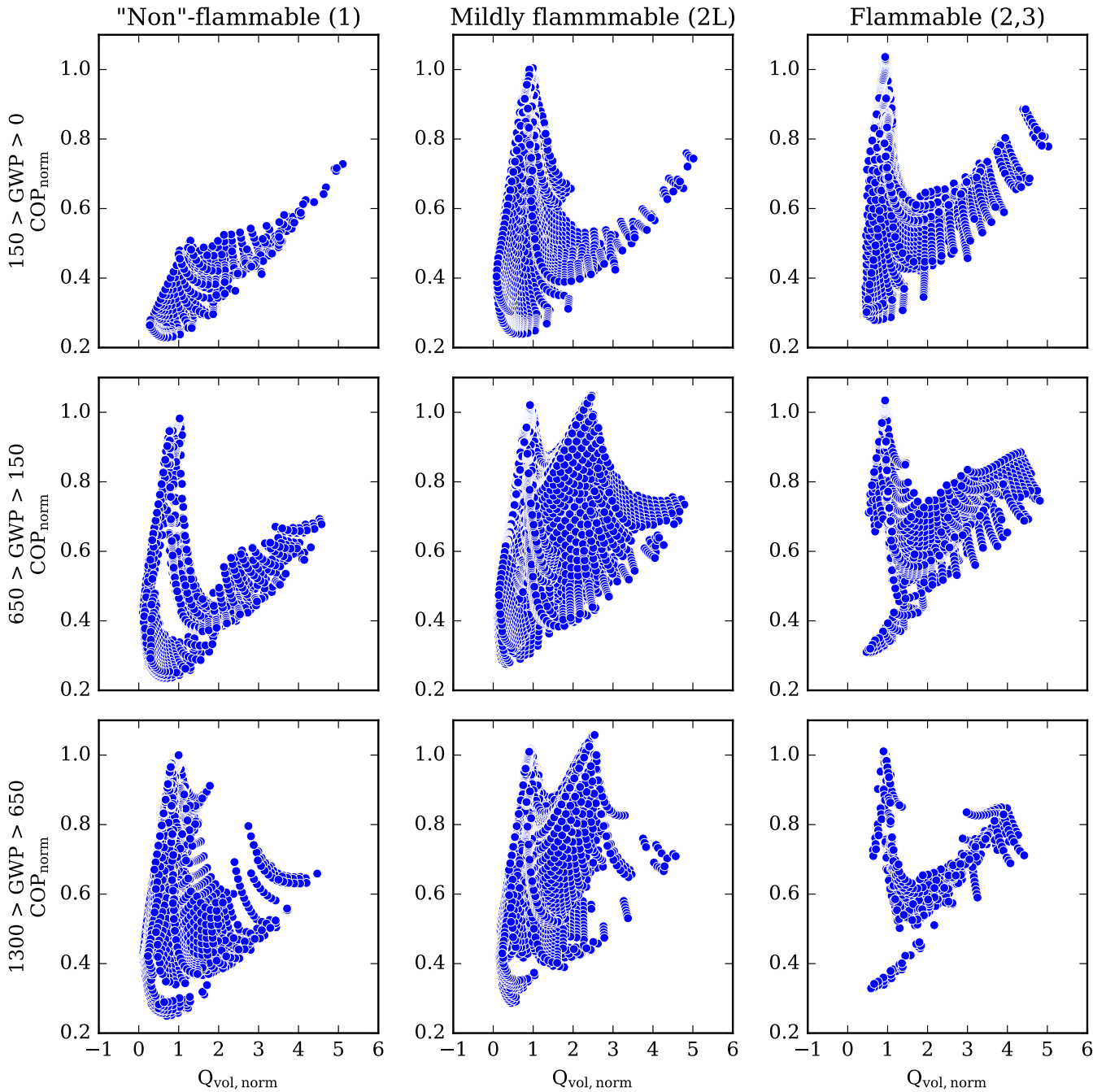


Figure 4: An overview of the cycle figures of merit for the binary and ternary blends studied, divided into bins of GWP and estimated flammability. The "best" bin is at the upper left, and the bins moving towards the lower right are worse according to our objective functions. Values of the volumetric capacity and COP are normalized by the value for the baseline R-134a system.

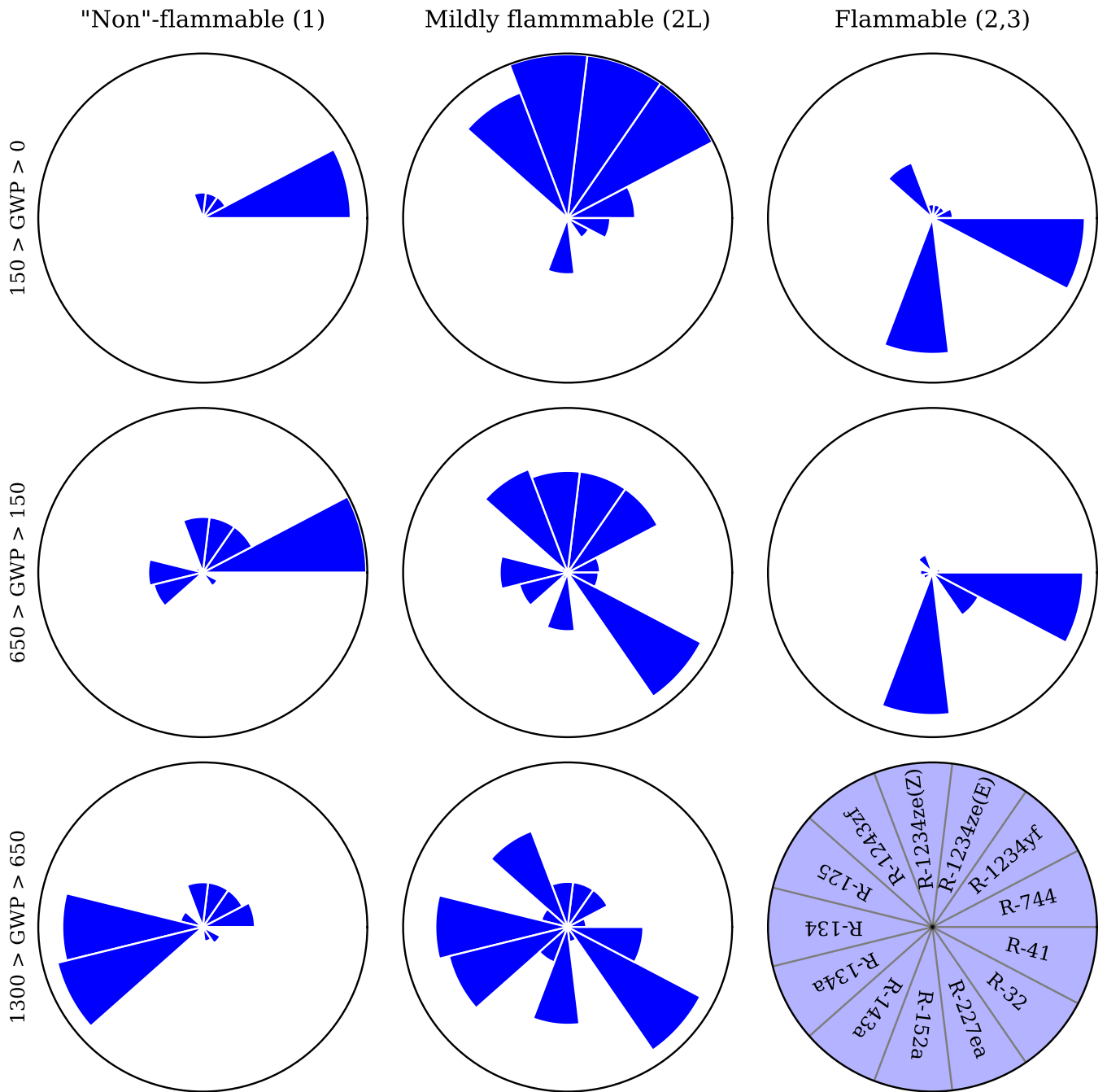


Figure 5: Radial histograms showing the prevalence of each component in each of the bins. The key in the lower right corner is aligned with the radial histograms in each bin.

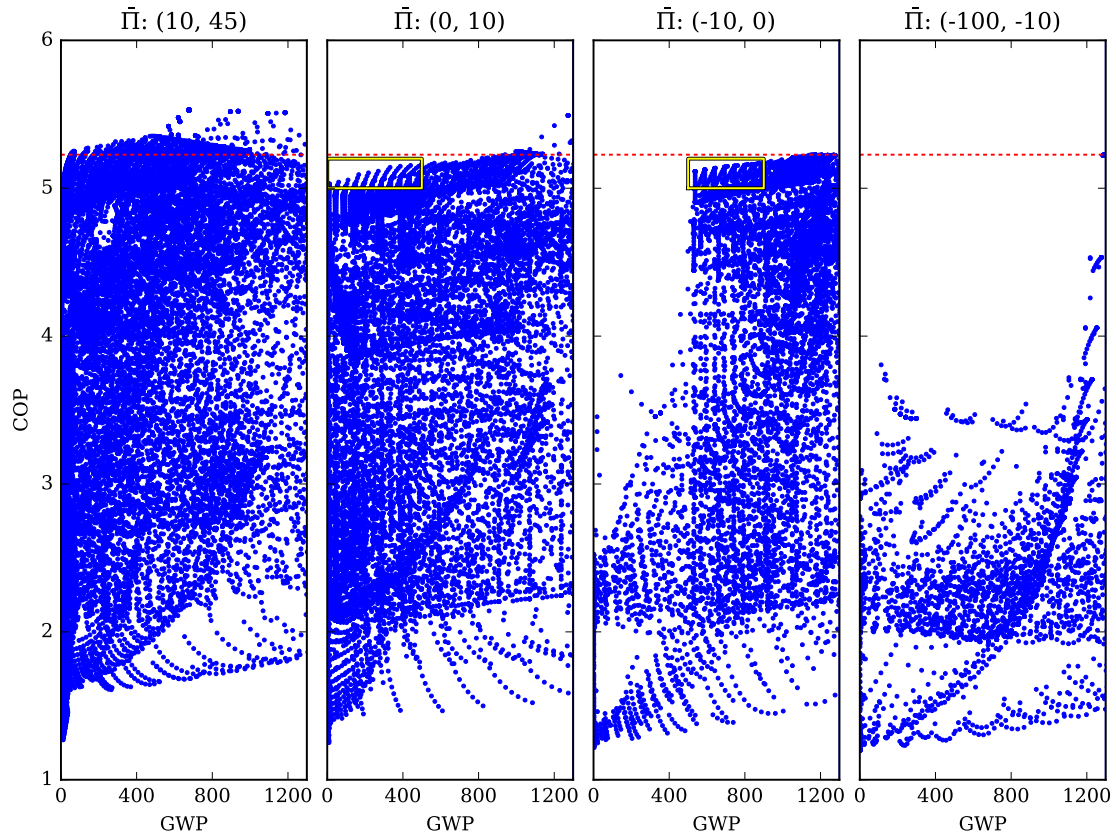


Figure 6: Overview of cycle simulation results sorted into bins of estimated flammability. The flammability increases moving from right to left; the right-most bin is predicted to be non-flammable. The red dashed line indicates the COP of the R-134a baseline system, and the yellow boxes correspond to the zoomed-in views shown in Fig. 7

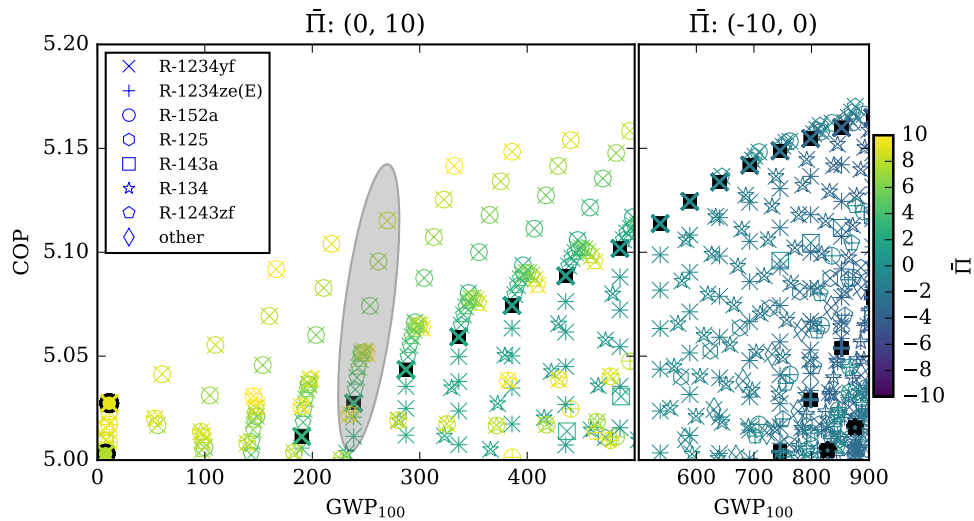


Figure 7: Insets for flammability from Fig. 6 showing the blends with COP > 5.0 for two "bins" of flammability; the left panel shows blends that are "borderline flammable" and the right panel shows blends that are estimated to be "nonflammable." The symbols plot the COP simulated with the simple vapor compression cycle model versus the GWP of the blend. The different symbols indicate the components of the blend; the majority of the blends shown have R-134a as a component, and the shapes indicate the other component(s). For example, the superposition of an "x" and a "O" indicates a R-134a/1234yf/152a ternary blend. The heavy black symbols denote the R-134a/1234yf, R-134a/1234ze(E), and R-134a/134 binaries. The colors of the symbols indicate the flammability index estimated by the method described in Section 3.2; the color key is at the right side of the plot. The points inside the shaded oval are discussed in the text.

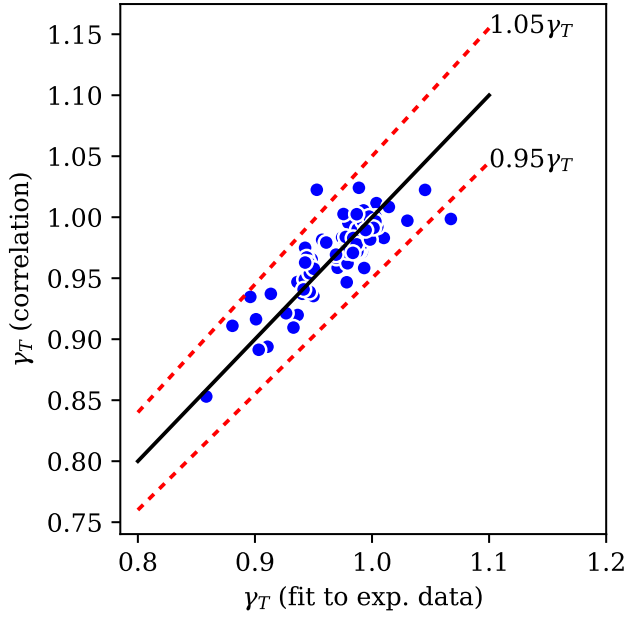


Figure 8: The estimated (from correlation) and experimentally fit values of the mixing parameter  $\gamma_T$  from the estimation scheme of Lemmon and McLinden (2001).

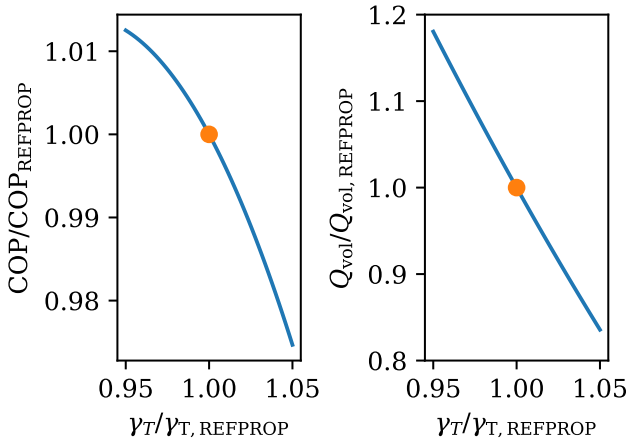


Figure 9: The sensitivity of model results to perturbation of the interaction parameter  $\gamma_T$  for the equimolar binary mixture of R-134a/1234yf around the nominal value of  $\gamma_{T, \text{REFPROP}} = 0.985$ . The circular markers indicate the nominal values in REFPROP 10.0.

## 4. Detailed Cycle Simulations

### 4.1. Model Description

We performed detailed cycle simulations on the “best” blends described in Section 3.5 with the public-domain CYCLE\_D-HX model (Brown et al., 2017). In contrast to the simplified vapor compression cycle model, which requires refrigerant saturation temperatures in the evaporator and condenser as inputs, CYCLE\_D-HX establishes saturation temperatures in the heat exchangers using the specified temperatures profiles of the heat source and heat sink (*i.e.*, the conditioned and outdoor air) and the mean effective temperature differences ( $\Delta T_{\text{hx}}$ ) in the evaporator and condenser. This representation of heat exchangers facilitates the inclusion of both thermodynamic and transport properties in cycle simulations (Brown et al., 2002a,b; Brignoli et al., 2017). The evaporator and condenser can be counterflow, crossflow, or parallel flow, although only cross-flow is simulated here.

During the iteration procedure, CYCLE\_D-HX calculates  $\Delta T_{\text{hx}}$  for each heat exchanger from (Domanski and McLinden, 1992):

$$\frac{1}{\Delta T_{\text{hx}}} = \frac{Q_1}{Q_{\text{hx}}\Delta T_1} + \frac{Q_2}{Q_{\text{hx}}\Delta T_2} + \dots = \frac{1}{Q_{\text{hx}}} \sum_i \frac{Q_i}{\Delta T_i} \quad (20)$$

In this equation,  $\Delta T_{\text{hx}}$  is a harmonic mean weighted with the fraction of heat transferred in individual sections of the heat exchanger, based on the assumption of a constant overall heat-transfer coefficient throughout the heat exchanger. Each term represents the contribution of a heat exchanger section. At the outset, the model calculates  $\Delta T_{\text{hx}}$  based on sections corresponding to the sub-cooled liquid, two-phase, and superheated regions. Then, the model bisects each section and uses Eq. (20) to calculate a new value of  $\Delta T_{\text{hx}}$ . The model repeatedly bisects each subsection until the  $\Delta T_{\text{hx}}$  obtained from two consecutive evaluations agree within a convergence parameter.

As an alternative to specifying  $\Delta T_{\text{hx}}$ , the heat exchangers can be characterized by the overall heat conductance  $UA_{\text{hx}} = 1/R_{\text{hx}}$  ( $R_{\text{hx}}$  being the total resistance to heat transfer in the heat exchanger). In this case, the model calculates the corresponding  $\Delta T_{\text{hx}}$  from the basic heat-transfer relation,  $\Delta T_{\text{hx}} = Q_{\text{hx}}/UA_{\text{hx}}$ , where  $Q_{\text{hx}}$  is the product of refrigerant mass flow rate and enthalpy change in the evaporator or condenser, as appropriate. The representation of heat exchangers by their  $UA_{\text{hx}}$  allows for inclusion of refrigerant heat transfer and pressure drop characteristics in comparable evaluations of different refrigerants. For this purpose, CYCLE\_D-HX considers  $R_{\text{hx}}$  as the summation of the resistance on the refrigerant side ( $R_r$ ), and combined resistances of the heat exchanger material and heat-transfer-fluid (HTF) side, ( $R_{\text{tube}} + R_{\text{HTF}}$ )

$$R_{\text{hx}} = R_r + (R_{\text{tube}} + R_{\text{HTF}}) \quad (21)$$

$$R_r = 1/(\alpha_r \cdot A_r) \quad (22)$$

where  $\alpha_r$  is the refrigerant heat-transfer coefficient in  $\text{W}\cdot\text{m}^2\cdot\text{K}^{-1}$  and  $A_r$  is the surface area on the refrigerant side in  $\text{m}^2$ .

The refrigerant heat-transfer resistance  $R_r$  varies with operating conditions and the refrigerant, but the other resistances ( $R_{\text{tube}} + R_{\text{HTF}}$ ) are assumed to be constant. Their combined value can be calculated from  $UA_{\text{hx}}$ ,  $\alpha_r$ , and  $A_r$  values during a simulation run for the “reference” refrigerant, for which the heat exchanger’s  $\Delta T_{\text{hx}}$  are known from laboratory measurements and were provided as input. CYCLE\_D-HX calculates ( $R_{\text{tube}} + R_{\text{HTF}}$ ) for the evaporator and condenser within this “reference run” and stores their values for use in subsequent simulation runs for calculation of  $UA_{\text{hx}}$  characterizing the heat exchangers with a new refrigerant or operating conditions.

CYCLE\_D-HX requires the following operational input data for the “reference run”: HTF inlet and outlet temperatures for the evaporator and condenser;  $\Delta T_{\text{hx}}$  for the evaporator and condenser (to achieve the measured evaporator and condenser saturation temperatures); evaporator superheat and pressure drop; and condenser subcooling and pressure drop. Additional “reference run” inputs include compressor isentropic and volumetric efficiencies, and electric motor efficiency. Heat exchanger geometry inputs include the tube inner diameter and length, the number of refrigerant circuits, and the number of tubes per circuit.

CYCLE\_D-HX also optimizes the coil circuiting in the evaporator and condenser to maximize the system’s COP. This option represents a design environment where the HTF and the number of refrigerant tubes remain constant, but the tube connections and number of refrigerant circuits can be changed. A smaller number of circuits results in a higher refrigerant mass flux, which brings the benefit of improved heat transfer and the penalty of increased pressure drop. Because of these two opposing trends, an optimum refrigerant mass flux exists. Typically, a high-pressure refrigerant will benefit from a smaller number of circuits than a low-pressure refrigerant because a high-pressure refrigerant realizes a lower drop of saturation temperature for a given pressure drop (Brignoli et al., 2017). Note that this analysis and optimization are applicable to systems with heat exchangers implementing forced-convection heat transfer (as opposed to pool-boiling and space condensation). Considering that all refrigerants are evaluated at the same system capacity as the reference fluid (the same heat flux through the evaporator), a necessary condition for a fair evaluation (McLinden and Radermacher, 1987), by using the optimization option, CYCLE\_D-HX provides information on the relative performance potential of refrigerants operating in systems with forced-convection refrigerant heat transfer (e.g., systems with serpentine air-to-refrigerant heat exchangers.)

### 4.2. Simulation Results

The series of CYCLE\_D-HX simulations of the 23 “best” blends started with R-134a simulations, which served as

Table 2: Detailed results from CYCLE\_D-HX ( $\bar{\Pi}$ : normalized flammability metric from Eq. (19) with initial temperature of 60 °C, and mole fraction of H<sub>2</sub>O in the air of 0.014)

| Blend components                        | Composition (molar) | GWP <sub>100</sub> | COP/COP <sub>R-134a</sub> | $Q_{vol}/Q_{vol,R-134a}$ | $\bar{\Pi}$ |
|---|---------------------|--------------------|---------------------------|--------------------------|-------------|
| <i>Class 1 nonflammable (predicted)</i> |                     |                    |                           |                          |             |
| R-134a/1234yf                           | 0.44/0.56           | 537                | 0.987                     | 1.025                    | -0.1        |
| R-134a/1234yf                           | 0.468/0.532 †       | 573                | 0.988                     | 1.027                    | -0.4        |
| R-134a/1234yf/134                       | 0.48/0.48/0.04      | 633                | 0.987                     | 0.975                    | -1.1        |
| R-134a/1234yf/1234ze(E)                 | 0.52/0.32/0.16      | 640                | 0.987                     | 0.989                    | -1.2        |
| R-134a/1234yf                           | 0.52/0.48           | 640                | 0.989                     | 1.029                    | -1.2        |
| R-134a/1234yf/134                       | 0.4/0.44/0.16       | 665                | 0.986                     | 0.958                    | -1.3        |
| R-134a/125/1234yf                       | 0.44/0.04/0.52      | 676                | 0.985                     | 1.049                    | -1.5        |
| R-134a/227ea/1234yf                     | 0.40/0.04/0.56      | 681                | 0.984                     | 1.007                    | -1.5        |
| R-134a/1234ze(E)                        | 0.60/0.40           | 745                | 0.988                     | 0.908                    | -2.4        |
| R-134a/1234yf                           | 0.60/0.40           | 745                | 0.990                     | 1.031                    | -2.4        |
| R-134a/1234ze(E)/1243zf                 | 0.60/0.36/0.04      | 750                | 0.990                     | 0.966                    | -1.5        |
| R-134a/1234yf/1234ze(E)                 | 0.64/0.2/0.16       | 799                | 0.990                     | 0.986                    | -3.0        |
| R-134a/152a/1234yf                      | 0.64/0.04/0.32      | 817                | 0.993                     | 1.023                    | -1.8        |
| R-134a/1234yf/134                       | 0.52/0.32/0.16      | 824                | 0.990                     | 0.966                    | -3.2        |
| R-134a/1234ze(E)                        | 0.68/0.32           | 852                | 0.991                     | 0.929                    | -3.7        |
| R-134a/1234yf/1243zf                    | 0.68/0.2/0.12       | 870                | 0.994                     | 1.020                    | -1.1        |
| <i>Class 2L flammable (predicted)</i>   |                     |                    |                           |                          |             |
| R-152a/1234yf                           | 0.08/0.92           | 8                  | 0.980                     | 0.957                    | 7.7         |
| R-134a/1234yf                           | 0.20/0.80           | 238                | 0.980                     | 0.996                    | 2.8         |
| R-134a/152a/1234yf                      | 0.20/0.16/0.64      | 270                | 0.987                     | 0.984                    | 8.7         |
| R-152a/1234yf/134                       | 0.16/0.48/0.36      | 417                | 0.984                     | 0.900                    | 7.5         |
| R-134a/1234yf                           | 0.36/0.64           | 436                | 0.985                     | 1.018                    | 1.0         |
| R-134a/1234yf/1243zf                    | 0.36/0.44/0.20      | 451                | 0.988                     | 1.004                    | 5.2         |
| R-134a/152a/1234yf                      | 0.36/0.20/0.44      | 496                | 0.994                     | 0.994                    | 8.3         |

†: This mixture corresponds to the nominal composition of the blend R-513A

the "reference" refrigerant. For this purpose, we established a 10 kW R-134a system, with operating parameters approximating those used in the simplified cycle simulations: the same evaporator outlet superheat (5 K), condenser exit subcooling (7 K) and compressor efficiency (0.7) were used; however, refrigerant pressure drop (corresponding to 2 K drop in saturation temperature) was imposed in the heat exchangers (as opposed to the compressor suction and discharge sides), and average two-phase temperatures in the heat exchangers were considered as opposed to the dew-point temperature (evaporator) and bubble-point temperature (condenser). Among the input not used for simplified cycle simulation but required by CYCLE\_D-HX, the values for compressor volumetric efficiency and electric motor efficiency were 1.0; the evaporator and condenser were cross-flow heat exchangers, which operated with inlet/outlet HTF temperatures of 25.0 °C/15.0 °C and 31.0 °C/35.0 °C, respectively. Both heat exchangers used tubes with an enhanced inner surface, with inner diameters of 0.00914 m (evaporator) and 0.00772 m (condenser). In addition to the inner tube diameters, the size of the refrigerant heat-transfer area in the heat exchangers was established by the specified "reference" number of tubes per circuit, 10 and 12; the number of circuits, 7 and 5; and the tube length, 0.8 m and 1.32 m; for the evaporator and condenser, respectively. Note that CYCLE\_D-HX optimized the last two parameters within the optimization process of refrigerant circuitry for each blend.

The first simulation was executed for a R-134a system with unoptimized heat exchangers. It required inputs of  $\Delta T_{\text{hx}}$  for the evaporator and condenser, which were 9.0 K and 6.5 K, respectively. The second simulation involved optimization of heat exchangers' circuitry to attain the maximum COP of the R-134a system. The performance of this optimized R-134a system became the reference for normalization of COP and  $Q_{\text{vol}}$  of the 23 blends (Table 2).

Table 2 presents GWP and simulation results for the 23 blends. For the group predicted to be nonflammable, the normalized values for COP and  $Q_{\text{vol}}$  were in the 0.984 – 0.994 and 0.908 – 1.049 range, respectively, with the GWP values ranging from 537 to 870. The main component of all of these blends is R-134a. The other components are the HFOs R-1234yf, R-1234ze(E), and R-1243zf and HFCs R-152a and R-134; R-125 and R-227ea appear at a low concentration in one blend each. Table 2 includes the mildly flammable group to accommodate the uncertainty of the flammability prediction method. For this group, the GWP values range from 8 to 496, and the normalized COP ranges from 0.980 to 0.994. The normalized  $Q_{\text{vol}}$  of the blends in this group are in the range 0.900 – 1.018. These blends comprise R-134a as the main component along with R-1234yf, and R-152a; R-134 and R-1243zf appear in one blend each.

Keeping in mind that the main goal of this study was to find a nonflammable, low-GWP replacement with a comparable COP and  $Q_{\text{vol}}$  of that for R-134a in an air-

conditioning application, the lowest GWP among the suitable nonflammable blends is 537, a 54% reduction in GWP compared with R-134a. The blend R-134a/1234yf, with molar composition (0.468/0.532) and GWP = 573, was predicted to be just barely on the non-flammable side of the 1/2L boundary, with calculated normalized flammability index for this mixture of  $\bar{\Pi} = -0.4$ . This blend has an ASHRAE 34 classification of class 1 (non-flammable).

For the group with a probable 2L flammability classification according to the ASHRAE 34 standard, there are options that yield efficiency near that of the baseline R-134a system with GWP of 8 and 4.3 % lower  $Q_{\text{vol}}$ . If a more moderate reduction in GWP is acceptable, there are higher-pressure low-GWP options with R-32 that attain a similar COP as R-134a with a more than doubled  $Q_{\text{vol}}$  (i.e., the fluids making up the second COP maximum shown in the middle panel of Fig. 4).

The twenty-three blends identified in Table 2 can be compared with existing blends in ASHRAE Standard 34. For example, the R-451 and R-513 designation groups of Standard 34 are represented by five R-134a/1234yf blends in the table, and R-450A is similar to two zeotropes of R-134a/1234ze(E) in the table. In addition, there are four existing non-flammable, low-toxicity blends (R-456A, R-460C, R-515A and R-515B) that are not similar to blends in the table. In all cases, however, the blends given in Table 2 have somewhat better predicted performance than the existing compounds listed in ASHRAE Standard 34, as determined by their combination of COP,  $Q_{\text{vol}}$ , GWP and  $\bar{\Pi}$ .

## 5. Uncertainty of Cycle Results

The uncertainty in the simulated cycle performance arises from several sources. The first source stems from the assumptions and idealizations made in the cycle models. Here, all fluids were simulated with the same assumptions, and we were concerned with relative difference between fluids. We estimated the uncertainty arising from this source based on the difference between the COP or  $Q_{\text{vol}}$  calculated by the simplified cycle model and the advanced cycle model discussed in Section 4 for the 23 blends calculated with both models. The average difference in COP was -1.5% and the average difference in  $Q_{\text{vol}}$  was -0.5%, and these reflect the degree to which the approximations made in the simplified model differed from the detailed model, but again these approximations were the same for all blends. The standard deviations of 0.8% in the COP difference and 2.2% in the  $Q_{\text{vol}}$  difference indicate the uncertainty associated with the screening of tens of thousands of blends (with the simplified model) compared to the more advanced cycle model. In other words, the screening study must, by necessity, use the simplified model, and it was these results that were used to select the "best" blends for further consideration with the advanced cycle model, which would give a more accurate representation of the true performance of a blend in actual equip-

ment. Any consistent difference between the two models for the different blends would not affect the relative ranking or choice of "best" blends. Any scatter in the COP or  $Q_{vol}$  differences (as characterized by the standard deviations) could affect the choice and must be considered as an uncertainty associated with the modeling.

The second source of uncertainty in the simulation results stemmed from refrigerant blend thermodynamic and transport properties. The thermodynamic properties are expressed in terms of an "equation of state" (EOS). For the 13 pure fluids considered here, high-accuracy EOS explicit in the Helmholtz energy were available and implemented in NIST REFPROP version 10.0 (Lemmon et al., 2018) for all but R-134; for R-134, a preliminary equation of state (of high accuracy) was employed. Thus, we consider the uncertainties in the thermodynamic properties of the pure fluids to be negligible for the purpose of this study.

The properties of a refrigerant blend are given by a combination of the equations of state for the constituent pure fluids in the blend plus additional EOS terms representing the mixture. The representation of a mixture is based on mixing coefficients for all pairs of the fluids in the mixture, and the most important interaction parameter is  $\gamma_T$  (Bell and Lemmon, 2016). For many of the blends simulated here these mixing coefficients were based on the estimation method of Lemmon and McLinden (2001). The uncertainty in this method is indicated in Fig. 8, which shows the predicted versus experimentally-based values of the mixing coefficient  $\gamma_T$ . This figure indicates an uncertainty in the mixing coefficient of  $0.05\gamma_T$ . The method was developed largely with CFC, HCFC, and HFC blends, with also a few hydrocarbon-containing blends. Blends with HFOs show somewhat higher errors, and we take  $0.10\gamma_T$  as a conservative estimate for the uncertainty in a predicted value of the mixing parameter. For the binary interaction parameters of HFO-containing blends fitted to experimental measurements, the data are generally limited and we use an uncertainty for these mixtures in  $\gamma_T$  of  $0.02\gamma_T$ . We use a global value of  $0.05\gamma_T$  as an average value for the uncertainty in the mixing parameter. The propagation of this uncertainty to the calculated COP is shown in Fig. 9 for the case of the R-134a/1234yf blend. Here we calculated the COP with the simplified cycle model over a range of values for the mixing parameter corresponding to its uncertainty. The result is an uncertainty of 1.9 % in the COP. The corresponding uncertainty in  $Q_{vol}$  is larger, about 18 %, as shown in Fig. 9.

## 6. Conclusions

Our search for nonflammable low-GWP replacements for R-134a in an air-conditioning system yielded several blends with COP and  $Q_{vol}$  similar to those of R-134a. The GWP of the identified nonflammable blends were in the 537 - 870 range. Among the mildly flammable (2L) blends, GWP reductions of more than a factor of 100 relative to R-134a were identified.

The study was limited to binary and ternary blends formed from a set of 13 pure fluids currently available in NIST REFPROP (Lemmon et al., 2018). Four-component blends from the same set of fluids were also simulated, although no such blends were superior to the two- and three-component blends. Additional pure fluids, such as those identified by McLinden et al. (2017), should be considered once sufficient experimental data become available to build the thermodynamic equations of state and mixture models required to implement them into REFPROP.

The COP and  $Q_{vol}$  values calculated from the CYCLE\_D-HX model present the relative performance potential of the considered fluids in a system with air-to-refrigerant heat exchangers. Experimental validation of these findings and predicted flammability classifications is merited.

Finally, flammability limits are generally device-dependent, so while the current estimation method can predict the behavior of a mixture in the ASTM E681 test protocol (for constituents which are chemically similar to those used to develop the model; i.e., hydrocarbons, HFCs, HFOs, etc.), the behavior of the mixtures in other flammability tests or actual full-scale configurations having more powerful ignition sources, clutter, turbulence, etc., may not be predicted as well. The relevance of the ASTM E681 classification for actual systems near the borderline of flammability should be experimentally verified.

## Acknowledgments

This work was supported by the U.S. Department of Defense, Strategic Environmental Research and Development Program (SERDP), project WP-2740.

## Supplemental Material

Available at:  
<https://doi.org/10.6084/m9.figshare.8171342>.

It includes:

- The Python code that was used to run the cycle calculations, and the code used to call Cantera to carry out the flammability estimation calculations
- The raw results from each simplified cycle run, in comma-separated format
- The inputs and outputs for the calculations of CYCLE-D\_HX
- A table of cycle evaluations for the ASHRAE 34 blends (when possible)

ASHRAE, 2016. ANSI/ASHRAE Standard 34-2016 Designation and Safety Classification of Refrigerants.

Bell, I.H., Domanski, P., Linteris, G., McLinden, M., 2018. Evaluation of binary and ternary refrigerant blends as replacements for R134a in an air-conditioning system, in: 17th International Refrigeration and Air Conditioning Conference at Purdue, July 9-12, 2018, p. 2110.

- Bell, I.H., Lemmon, E.W., 2016. Automatic Fitting of Binary Interaction Parameters for Multi-fluid Helmholtz-Energy-Explicit Mixture Models. *J. Chem. Eng. Data* 61, 3752–3760. doi:10.1021/acs.jced.6b00257.
- Bell, I.H., Wronski, J., Quoilin, S., Lemort, V., 2014. Pure and Pseudo-pure Fluid Thermophysical Property Evaluation and the Open-Source Thermophysical Property Library CoolProp. *Ind. Eng. Chem. Res.* 53, 2498–2508. doi:10.1021/ie4033999.
- Brignoli, R., Brown, J.S., Skye, H.M., Domanski, P.A., 2017. Refrigerant performance evaluation including effects of transport properties and optimized heat exchangers. *Int. J. Refrig* 80, 52–65. doi:10.1016/j.ijrefrig.2017.05.014.
- Brown, J., 2012. Introduction to Alternatives for High-GWP HFC Refrigerants, in: ASHRAE/NIST Refrigerants Conference, October 29–30, 2012, Gaithersburg, MD.
- Brown, J., Kim, Y., Domanski, P., 2002a. Evaluation of Carbon Dioxide as R22 Substitute for Residential Conditioning. *ASHRAE Trans.* 108, 954–963.
- Brown, J.S., Brignoli, R., Domanski, P.A., 2017. CYCLE\_D-HX: NIST vapor compression cycle model accounting for refrigerant thermodynamic and transport properties, version 1.0, user's guide. Technical Note 1974. NIST. URL: <https://www.nist.gov/services-resources/software/cycled-hx-nist-vapor-compression-cycle-model-accounting-refrigerant>, doi:10.6028/nist.tn.1974.
- Brown, J.S., Yana-Motta, S.F., Domanski, P.A., 2002b. Comparative analysis of an automotive air conditioning systems operating with CO<sub>2</sub> and R134a. *Int. J. Refrig.* 25, 19–32. doi:10.1016/s0140-7007(01)00011-1.
- Domanski, P.A., McLinden, M.O., 1992. A simplified cycle simulation model for the performance rating of refrigerants and refrigerant mixtures. *Int. J. Refrig* 15, 81–88. doi:10.1016/0140-7007(92)90031-o.
- Gaurav, Kumar, R., 2018. Computational energy and exergy analysis of R134a, R1234yf, R1234ze and their mixtures in vapour compression system. *Ain Shams Engineering Journal* 9, 3229–3237. doi:10.1016/j.asej.2018.01.002.
- Goodwin, D.G., Moffat, H.K., Speth, R.L., 2017. Cantera: An Object-oriented Software Toolkit for Chemical Kinetics, Thermodynamics, and Transport Processes. <http://www.cantera.org>. doi:10.5281/zenodo.170284. version 2.3.0.
- Kondo, S., Takizawa, K., Tokuhashi, K., 2012. Effects of temperature and humidity on the flammability limits of several 2L refrigerants. *J. Fluorine Chem.* 144, 130–136. doi:10.1016/j.jfluchem.2012.08.004.
- Lemmon, E.W., Bell, I.H., Huber, M.L., McLinden, M.O., 2018. NIST Standard Reference Database 23: Reference Fluid Thermodynamic and Transport Properties-REFPROP, Version 10.0, National Institute of Standards and Technology. <http://www.nist.gov/srd/nist23.cfm>.
- Lemmon, E.W., McLinden, M.O., 2001. Method for Estimating Mixture Equation of State Parameters, in: *Thermophysical Properties and Transfer Processes of New Refrigerants*, Paderborn, Germany.
- Linteris, G., Bell, I., McLinden, M., Domanski, P., 2018. An Empirical Model For Refrigerant Flammability Based On Molecular Structure and Thermodynamics, in: *17th International Refrigeration and Air Conditioning Conference at Purdue*, July 9–12, 2018, p. 2694.
- Linteris, G., Bell, I.H., McLinden, M.M., 2019, under revision. An Empirical Model for Refrigerant Flammability Based on Molecular Structure and Thermodynamics. *Int. J. Refrig.*
- Llopis, R., Sánchez, D., Cabello, R., Catalán-Gil, J., Nebot-Andrés, L., 2017. Experimental analysis of R-450A and R-513A as replacements of R-134a and R-507A in a medium temperature commercial refrigeration system. *Int. J. Refrig* 84, 52–66. doi:10.1016/j.ijrefrig.2017.08.022.
- McLinden, M., Radermacher, R., 1987. Methods for comparing the performance of pure and mixed refrigerants in the vapour compression cycle. *Int. J. Refrig.* 10, 318–325. doi:10.1016/0140-7007(87)90117-4.
- McLinden, M.O., Brown, J.S., Brignoli, R., Kazakov, A.F., Domanski, P.A., 2017. Limited options for low-global-warming-potential refrigerants. *Nat. Commun.* 8, 14476. doi:10.1038/ncomms14476.
- Mota-Babiloni, A., Makhnatch, P., Khodabandeh, R., Navarro-Esbrí, J., 2017. Experimental assessment of R134a and its lower GWP alternative R513A. *Int. J. Refrig* 74, 682–688. doi:10.1016/j.ijrefrig.2016.11.021.
- Mota-Babiloni, A., Navarro-Esbrí, J., Barragán-Cervera, Á., Molés, F., Peris, B., 2015. Experimental study of an R1234ze(E)/R134a mixture (R450A) as R134a replacement. *Int. J. Refrig* 51, 52–58. doi:10.1016/j.ijrefrig.2014.12.010.
- Myhre, G., Shindell, D., Bréon, F.M., Collins, W., Fuglestedt, J., Huang, J., Koch, D., Lamarque, J.F., Lee, D., Mendoza, B., Nakajima, T., Robock, A., Stephens, G., Takemura, T., Zhang, H., 2013. Anthropogenic and Natural Radiative Forcing, in: Stocker, T., Qin, D., Plattner, G.K., Tignor, M., Allen, S.K., Boschung, J., Nauels, A., Xia, Y., Bex, V., Midgley, P. (Eds.), *Climate Change 2013: The Physical Science Basis. Contribution of Working Group I to the Fifth Assessment Report of the Intergovernmental Panel on Climate Change*. Cambridge University Press, Cambridge, United Kingdom and New York, NY, USA., pp. 659–740.
- Sánchez, D., Cabello, R., Llopis, R., Arauzo, I., Catalán-Gil, J., Torrella, E., 2017. Energy performance evaluation of R1234yf, R1234ze(E), R600a, R290 and R152a as low-GWP R134a alternatives. *International Journal of Refrigeration* 74, 269–282. doi:10.1016/j.ijrefrig.2016.09.020.
- Takahashi, A., Urano, Y., Tokuhashi, K., Kondo, S., 2003. Effect of vessel size and shape on experimental flammability limits of gases. *J. Hazard. Mater.* 105, 27–37. doi:10.1016/j.jhazmat.2003.07.002.
- UNEP, 2016. Amendment to the Montreal Protocol on Substances that Deplete the Ozone Layer, Kigali, 15 October 2016. URL: <https://treaties.un.org/doc/Publication/CN/2016/CN.872.2016-Eng.pdf>.
- Wang, C.C., 2014. System performance of R-1234yf refrigerant in air-conditioning and heat pump system – An overview of current status. *Appl. Therm. Eng.* 73, 1412–1420. doi:10.1016/j.applthermaleng.2014.08.012.